Processes determining the marine alkalinity and calcium carbonate saturation state distributions

Carter, B. R.[1], J. R. Toggweiler[2], R. M. Key[1], and J. L. Sarmiento[1]

Brendan Carter (brcarter@princeton.edu)

J.R. Toggweiler (Robbie.Toggweiler@noaa.gov)

Robert M. Key (key@princeton.edu)

Jorge L. Sarmiento (jls@princeton.edu)

[1] Atmospheric and Oceanic Sciences Program, Princeton University, Princeton, NJ, USA
[2] Geophysical Fluid Dynamics Laboratory, National Oceanic and Atmospheric Administration, P.O. Box 308, Princeton NJ, 08542, USA

Abstract

We introduce a composite tracer for the marine system, $Alk*$, that has a global distribution primarily determined by $CaCO_3$ precipitation and dissolution. $Alk*$ is also affected by riverine alkalinity from dissolved terrestrial carbonate minerals. We estimate that the Arctic receives approximately twice the riverine alkalinity per unit area as the Atlantic, and eight times that of the other oceans. Riverine inputs broadly elevate $Alk*$ in the Arctic surface and particularly near river mouths. Strong net carbonate precipitation results in low $Alk*$ in subtropical gyres, especially in the Indian and Atlantic Oceans. Upwelling of dissolved $CaCO_3$ rich deep water elevates Northern Pacific and Southern Ocean $Alk*$. We use the $Alk*$ distribution to estimate the variability of the calcite saturation state resulting from $CaCO_3$ cycling and other processes. We show that regional differences in surface calcite saturation state are due primarily to the effect of temperature differences on CO_2 solubility and, to a lesser extent, differences in freshwater content and air-sea disequilibria. The variations in net calcium carbonate cycling revealed by $Alk*$ play a comparatively minor role in determining the calcium carbonate saturation state.

1. Introduction

Our goal is to use high-quality total alkalinity (A_T) observations to examine the effects of calcium carbonate cycling on marine A_T and calcium carbonate saturation states. This study is motivated in part by ocean acidification. With marine calcite saturation states decreasing due to anthropogenic carbon uptake (Orr et al., 2005), it is important to understand the degree to which carbonate cycling impacts the calcium carbonate saturation state.

Carbonate saturation state is a measure of how supersaturated seawater is with respect to

24   a given mineral form of calcium carbonate. It is expressed for calcite as the ratio Ω_C between

25   the product of Ca^{2+} and CO_3^{2-} ion concentrations and the calcite thermodynamic equilibrium

26   solubility product. Values of Ω_C greater than one indicate calcite precipitation is favored

27   thermodynamically over calcite dissolution, and the reverse is true for values less than one.

28   Marine calcium carbonate cycling includes both internal and external calcium carbonate

29   sources and sinks. Internal cycling refers to net formation of 67-300 Tmoles A_T yr^{-1} worth of

30   calcium carbonate in the surface ocean (Berelson et al., 2007) and net dissolution of most of this

31   calcium carbonate at depth. External marine carbonate cycling refers to inputs of carbonate

32   minerals dissolved in rivers, sediment pore waters, hydrothermal vent fluids, and submarine

33   groundwater discharge, and to loss due to biogenic carbonate mineral burial and authigenic

34   mineralization in sediments. Rivers add 33 Tmoles A_T yr^{-1} worth of dissolved bicarbonate to the

35   ocean (Cai et al., 2008). Wolery and Sleep (1988) estimate that hydrothermal vents add an

36   additional 6.6 Tmoles A_T yr^{-1}, though deVilliers (1998) argues the hydrothermal contribution

37   may be as high as 30 Tmoles A_T yr^{-1}. Submarine groundwater discharge is poorly constrained,

38   but is thought to exceed riverine inputs in some areas (Moore, 2010).

39   We investigate calcium carbonate cycling using the global A_T distribution in a dataset we

40   created by merging the PACIFICA (Suzuki et al., 2013), GLODAP, and CARINA discrete data

41   products (Key et al. 2004; 2010; Velo et al., 2009). We have combined and gridded these data

42   products using methods detailed in Supplementary Materials document SA. We use our gridded

43   dataset in our calculations to limit sampling biases and to enable us to make volume-weighted

44   mean property estimates.

45   Dickson (1981) defines total alkalinity as the concentration excess "of proton acceptors

46   formed from weak acids ($pK \leq 4.5$) relative to proton donors (weak bases with $pK > 4.5$)" at a

47   reference temperature, pressure, and ionic strength. A_T can be thought of as a measure of how

48   well buffered seawater is against changes in pH. This operational definition gives A_T (expressed

49   in mol kg^{-1}) several properties that make it an especially useful carbonate system parameter for

50   examining carbonate cycling:

51   1. It mixes conservatively,

52   2. … and is therefore diluted and concentrated linearly by evaporation and precipitation.

53   3. It responds in predictable ways to calcium carbonate cycling.

54   4. … as well as organic matter formation and remineralization.

55   5. It is not changed by air-sea exchange of heat or carbon dioxide.

56   6. It is however affected by anaerobic redox reactions (Chen, 2002).

57   We are primarily interested in calcium carbonate cycling, item 3 in our list. In section 2 of this

58   paper we therefore define a tracer we call *Alk** that removes the majority of the influences of

59   organic matter cycling (item 4), freshwater cycling (item 2), and non-sedimentary anaerobic

60   redox reactions (item 6) while still mixing conservatively, remaining insensitive to gas exchange,

61   and responding to calcium carbonate cycling. In section 3 we discuss processes that govern the

62   *Alk** distribution globally, by ocean basin, and regionally. In section 4 we define a metric to

63   quantify the influence of various processes on the marine calcite saturation state. We use this

64   metric with our gridded dataset and *Alk** to determine the relative importance of the various

65   controls on calcite saturation state in the ocean and at the ocean surface. We summarize our

66   findings in section 5.

67

68   **2. The *Alk** tracer**

69   In defining *Alk**, we take advantage of the potential alkalinity (Brewer et al., 1975)

70   concept to remove the majority of the influence of organic matter cycling and denitrification, and

71   use a specific salinity normalization scheme (Robbins, 2001) to remove the influence of

72   freshwater cycling. We detail the *Alk** definition and the reasoning behind it in this section.

73   The influence of organic matter cycling on A_T is due primarily to the biologically-driven

74   marine nitrogen cycle. Nitrate uptake for anaerobic denitrification and the production of amino

75   acids occurs in a ~1:1 mole ratio with the release of molecules that increase A_T (Chen, 2002).

76   Similarly, nitrate from fixation of nitrogen gas and remineralization of amino nitrogen is released

77   in a 1:1 mole ratio with acids that titrate away A_T (Wolf-Gladrow et al., 2007). This observation

78   led Brewer et al. (1975) to propose the idea of "potential alkalinity" as the sum of A_T and nitrate

79   with the aim of creating a tracer that responds to the cycling of calcium carbonates without

80   changing in response to organic matter cycling. Feely et al. (2002) since used a variant that

81   relies on the empirical relationship between dissolved calcium concentrations, A_T, and nitrate

82   determined by Kanamori and Ikegami (1982). This variant has the advantage of implicitly

83   accounting for the A_T changes created by the exchange of numerous other components of marine

84   organic matter besides nitrate (e.g. sulfate and phosphate). We thus use the ratio found by

85   Kanamori and Ikegami (1982) to define potential alkalinity (A_P).

86
$$A_P = A_T + 1.26 * [NO_3^-] \tag{1}$$

87   While the empirical Kanamori and Ikegami (1982) ratio of 1.26 may be specific to the elemental

88   ratios of the North Pacific, Wolf-Gladrow et al. (2007) provide a theoretical derivation from

89   Redfield ratios and obtain a similar value of 1.36.

90   The sensitivity of the A_T distribution to freshwater cycling is due primarily to the dilution

91   or concentration of the large background A_T fraction that does not participate in carbonate

92   cycling on timescales of ocean mixing. This background fraction behaves conservatively, so we

93 call it conservative potential alkalinity (A_P^C) and estimate it directly from salinity as:

$$A_P^C \equiv S \frac{\overline{A_P}}{\overline{S}}$$
(2)

95 Here, terms with a bar are reference values chosen as the mean value for those properties in the

96 top 20 meters of the ocean. We obtain a volume-weighted surface $\overline{A_P}$ (2305 µmol kg^{-1}) to $\overline{S}$

97 (34.71) ratio of 66.40 µmol kg^{-1} from our gridded dataset. The mean surface values are chosen

98 in an effort to best capture the impact of freshwater cycling where precipitation and evaporation

99 occur.

100   Robbins (2001) showed that subtracting an estimate of the conservative portion of a

101 tracer, such as A_P^C , produces a salinity-normalized composite tracer that mixes conservatively.

102 This scheme also retains the 2:1 change of A_T to dissolved inorganic carbon (C_T) with carbonate

103 cycling. We follow this approach in our definition of *Alk**. In Supplementary Materials

104 document SB we estimate this approach removes 97.5% of the influence of freshwater cycling

105 on potential alkalinity and reduces the influence of freshwater cycling on *Alk** to less than 1% of

106 the *Alk** variability. In Supplementary Materials document SC we demonstrate that *Alk** mixes

107 conservatively, and briefly contrast *Alk** to traditionally normalized potential alkalinity which

108 does not mix conservatively (Jiang et al., 2014).

109   In total, we define *Alk** as the deviation of potential alkalinity from A_P^C ,

$$Alk^* \equiv A_P - A_P^C$$
(3)

110
$$\equiv A_P - \frac{\overline{A_P}}{\overline{S}} S$$
(4)

$$\equiv A_P - 66.4 \times S$$
(5)

111 where *Alk** has the same units as A_T (µmol kg^{-1}). The *Alk** distribution is attributable primarily

112 to carbonate cycling plus the small (in most places) residual variation due to freshwater cycling

113   that is not removed by subtracting A_P^C. However, hydrothermal vent fluid and non-

114   denitrification anaerobic redox chemistry may substantively affect alkalinity distributions in

115   certain marine environments, and *Alk** distributions could not be attributed purely to internal and

116   external calcium carbonate cycling in these locations.

117   Mean global surface *Alk** is zero by definition, and thus *Alk** can have negative as well

118   as positive values. For reference, more than 95% of our gridded *Alk** dataset falls between –35

119   and 220 µmol kg^{-1}. Comparing gridded *Alk** to *Alk** from measurements suggests a standard

120   disagreement of order 10 µmol kg^{-1}. We adopt this number as an estimate of standard gridded

121   *Alk** error despite noting there are reasons to suspect that this value could be either an

122   underestimate (correlated errors) or an overestimate (we are directly comparing instantaneous

123   point measurements to estimates for annual averages for a grid cell).

124

125   **3. *Alk** distributions**

126   We consider *Alk** distributions globally, by ocean basin, and regionally in the context of

127   sources and sinks of the tracer both globally and regionally. We pay special attention to riverine

128   *Alk** because it is easily identified where it accumulates near river mouths.

129

130   *3.1 Global distribution of Alk**

131   Figure 1 maps surface *Alk** (top 50 m) at the measurement stations. We provide this

132   figure to show where we have viable *Alk** estimates and to demonstrate that our gridded data

133   product adequately captures the measured *Alk** distribution. Figure 2 maps gridded global

134   surface A_T, salinity, *Alk**, and phosphate distributions and masks the regions that are lacking data

135   in Fig. 1.

136   The similarity of the A_T (Fig. 2a) and salinity (Fig. 2b) distributions demonstrates the

137   strong influence of freshwater cycling on the surface marine A_T distribution (see also: Millero et

138   al. 1998, Jiang et al., 2014). The dissimilarity between $Alk*$ (Fig. 2c) and salinity (Fig. 2b)

139   suggests $Alk*$ removes the majority of this influence. The phosphate (Fig. 2d) and $Alk*$ (Fig. 2c)

140   distributions are similar at the surface. They are also similar at depth: Figures 3 and 4 show

141   zonally-averaged gridded depth sections of $Alk*$ and phosphate. $Alk*$ and phosphate

142   concentrations are low in the deep Arctic Ocean (Figs. 3d, and 4d), intermediate in the deep

143   Atlantic Ocean (Figs. 3a and 4a), and high in the deep North Pacific (Figs. 3b and 4b) and deep

144   North Indian (Figs. 3c and 4c) Oceans. $Alk*$ and phosphate distributions are similar because

145   similar processes shape them: the hard and soft tissue pumps transport A_T and phosphate,

146   respectively, from the surface to depth. The "oldest" water therefore has the highest net

147   phosphate and $Alk*$ accumulation. High surface phosphate and $Alk*$ in the Southern Ocean and

148   North Pacific in Figs. 2, 3, and 4 are due to upwelled old deep waters.

149   Several qualitative differences between $Alk*$ and phosphate distributions are visible in

150   Figs. 2c, 2d, 3, and 4. Surface phosphate is low in the Bay of Bengal and high in the Arabian

151   Sea (Fig. 2d), while the opposite is true for $Alk*$ (Fig. 2c). Also, $Alk*$ reaches its highest surface

152   concentration in the Arctic (Figs. 2c and 3d) where phosphate is not greatly elevated (Figs. 2d

153   and 4d). These surface differences are due to regional riverine $Alk*$ inputs (Section 3.3).

154   Another difference is that $Alk*$ reaches a maximum below 2000 m in all ocean basins except the

155   Arctic, while phosphate maxima are above 2000 m. We attribute the deeper $Alk*$ maxima to

156   deeper dissolution of calcium carbonates than organic matter remineralization. Finally, $Alk*$

157   values are higher in the deep Indian Ocean than in the deep Pacific. This is likely due to elevated

158   biogenic carbonate export along the coast of Africa and in the Arabian Sea (Sarmiento et al.,

159   2002; Honjo et al., 2008).

160

161   *3.2 Alk* by ocean basin*

162   In Fig. 5 we provide 2-D color histograms of discrete surface *Alk** and salinity

163   measurements for the five major ocean basins. Figure 5 also indicates a single volume-weighted

164   mean gridded *Alk** for each basin (in writing). We attribute the decrease in *Alk** as salinity

165   increases—especially visible in the low-salinity bins in the Arctic Ocean (Fig. 5d)—to mixing

166   between high-*Alk** low-salinity river water and low-*Alk** high-salinity open ocean water. Net

167   precipitation in the tropics and net evaporation in the subtropics widens the histograms across a

168   range of salinities and alkalinities without affecting *Alk** in Figs. 5a, 5b, and 5c. The *Alk**

169   elevation associated with upwelled water is most visible in Fig. 5e where Upper Circumpolar

170   Deep Water upwelling near the Polar Front results in high-frequency (i.e. warm colored)

171   histogram bins at high-*Alk**. Similarly, the high-frequency *Alk** bins in Fig. 5b with salinity

172   between 32.5 and 33.5 are from the North Pacific Subpolar Gyre, and are due to upwelled old

173   high-*Alk** water (cf. the Si* tracer in Sarmiento et al. (2004)). River water contributions can be

174   most easily seen in a scattering of low-frequency (cool colored) high-*Alk** and low-salinity bins

175   in the Arctic Ocean.

176   The surface Southern Ocean has the highest *Alk** followed by the Arctic and the Pacific.

177   The Indian and Atlantic have similar and low mean *Alk**. The high mean Southern Ocean *Alk**

178   is due to upwelling. The high mean Arctic surface *Alk** is due to riverine input. The Atlantic

179   and the Arctic together receive ~65% of all river water (Dai and Trenberth, 2002). We construct

180   a budget for terrestrial A_T sources to the various surface ocean basins using the following

181   assumptions:

182   1. the A_T of 25 large rivers are as given by Cai et al. (2008),

183   2. the volume discharge rates of 200 large rivers are as given by Dai and Trenberth

184   (2002),

185   3. groundwater and runoff enter each ocean in the same proportion as river water from

186   these 200 rivers,

187   4. the A_T of all water types that we do not know from assumption 1. is the 1100 μmol

188   kg^{-1} global mean value estimated by Cai et al. (2008), and

189   5. 40°N is the boundary between the Atlantic and the Arctic and 40°S is the boundary

190   between the Southern and the Atlantic Oceans (based upon the region of elevated

191   surface phosphate in Fig. 2d),

192   Our detailed budget is provided as Supplementary Materials file SD. We estimate 40% of

193   continentally derived A_T enters the Atlantic, 20% enters the Arctic, and 40% enters all remaining

194   ocean basins. These ocean areas represent 17%, 5%, and 78% of the total surface ocean area in

195   our gridded dataset respectively, so the Artic receives approximately twice as much riverine A_T

196   per unit area as the Atlantic, and 8 times the rest of the world ocean. The Atlantic has the lowest

197   open-ocean surface *Alk** value and low basin mean surface *Alk** despite the large riverine

198   sources. The large riverine A_T input must therefore be more than balanced by strong net calcium

199   carbonate formation. The Indian Ocean has comparably low mean surface *Alk** to the Atlantic,

200   but a smaller riverine source. Mean *Alk** is higher in the Pacific than the Atlantic and Indian,

201   even when neglecting the region north of 40°N as we do for the Atlantic (*Alk** = −16.5 μmol

202   kg^{-1} when omitted vs. −22.9 μmol kg^{-1} for the Atlantic and −22.2 μmol kg^{-1} for the Indian).

203   The difference between the Pacific and the other basins is significant when considering the large

204   number of grid cell *Alk** values averaged (> 6000 in the Atlantic), and the small estimated

205   uncertainty for each value (~10 μmol kg^{-1}). Considering the weak Pacific riverine input, this

206   suggests that, relative to other ocean basins, there are either larger *Alk** inputs from exchange

207   with other basins and deeper waters or smaller Pacific basin mean net calcium carbonate

208   formation.

209

210   *3.3 Riverine Alk* regionally*

211   For river water with negligible salinity, *Alk** equals the potential alkalinity. This

212   averages around 1100 μmol kg^{-1} globally (Cai et al., 2008), but is greater than 3000 μmol kg^{-1}

213   for some rivers (Beldowski et al., 2010). Evidence suggests that riverine A_T is increasing due to

214   human activities (Kaushal et al., 2013).

215   The most visible riverine *Alk** signals are in the Arctic due to the large riverine runoff

216   into this comparatively small basin and the confinement of this low-density riverine water to the

217   surface (Jones et al., 2008; Yamamoto-Kawai et al., 2009; Azetsu-Scott et al., 2010). Figure 3d

218   shows the high Arctic *Alk** plume is confined to the top ~200 m. Figure 1 shows that these high

219   *Alk** values extend along the coast of Greenland and through the Labrador Sea. *Alk** decreases

220   with increasing salinity in this region (Fig. 5d) due to mixing between the fresh high *Alk** surface

221   Arctic waters and the salty lower *Alk** waters of the surface Atlantic. Gascard et al. (2004a, b)

222   suggest that waters along the coast of Norway are part of the Norwegian Coastal Current, and

223   originate in the Baltic and North Seas where there are also strong riverine inputs (Thomas et al.,

224   2005).

225   Elevated *Alk** can also be seen in the Bay of Bengal with surface values ~100 μmol kg^{-1}

226   higher than those in the central Indian Ocean. This bay has two high A_T rivers that join and flow

227   into it, the Brahmaputra (A_T = 1114 μmol kg^{-1}) and the Ganges (A_T = 1966 μmol kg^{-1}) (Cai et al.,

228   2008). Figure 6b provides an *Alk** depth section for this region. The riverine *Alk** plume can be

229   clearly seen in the top 50 m. No similar increase is seen in the Arabian Sea (Fig. 6a) where the

230   Indus River (1681 μmol kg^{-1}) discharges only ~1/10th of the combined volume of the

231   Brahmaputra and the Ganges.

232   The Amazon River is the largest single riverine marine A_T source. This river has low A_T

233   (369 μmol kg^{-1} (Cai et al., 2008)), but has the largest water discharge volume of any river,

234   exceeding the second largest—the Congo—by a factor of ~5 (Dai and Trenberth, 2002).

235   Consequently, the Amazon discharges approximately 50% more A_T per year than the river with

236   the second largest A_T discharge, the Changjiang (Cai et al., 2008). The Amazon's influence can

237   be seen as a region of abnormally low salinity and A_T in Fig. 2a and b. Despite the high

238   discharge volume, the influence is only barely visible as a region of elevated *Alk** in Fig. 2c due

239   to the comparatively low Amazon *Alk**. However, the influence of the Amazon on *Alk** can be

240   seen in the seasonal *Alk** cycle in the Amazon plume. Figure 7 provides a map of *Alk** for this

241   region scaled to show the influence of this low *Alk** river in the Northern Hemisphere (a) winter

242   and (b) summer months. The higher *Alk** found for summer months is consistent with Amazon

243   discharge and A_T seasonality (Cooley et al., 2007) and Moore et al.'s (1986) radium isotope

244   based finding that Amazon River outflow comprises 20-34% of surface water in this region in

245   July compared to only 5-9% in December.

246

247   *3.4 Regional abiotic carbonate cycling*

248   The Red Sea portion of Fig. 6a is strongly depleted in *Alk**, and contains the lowest

249   single *Alk** measurement in our dataset, –247 μmol kg^{-1}. The GEOSECS expedition Red Sea

250   alkalinity measurements (Craig and Turekian, 1980) predate alkalinity reference materials

251   (Dickson et al., 2007), but are supported by more recent measurements (Silverman et al., 2007).

252   Like Jiang et al. (2014), we attribute low Red Sea *Alk** to exceptionally active calcium carbonate

253   formation. Brewer and Dyrssen (1985) provide seawater chemistry measurements from the

254   neighboring Persian Gulf that suggest strong calcium carbonate formation results in low *Alk**

255   there as well (< -240 µmol kg^{-1} along the Trucial Coast).

256   The Red Sea is one of the only regions where Ω_C is sufficiently high for abiotic

257   carbonate precipitation to significantly contribute to overall carbonate precipitation (Milliman et

258   al. 1969; Silverman et al., 2007). Notably, saturation state remains high at depth in the Red Sea

259   (see Section 4.2). In this region, biogenic aragonitic corals and pteropod shells are progressively

260   removed with depth in sediments, and pores left behind are filled in with high-magnesium calcite

261   cement (Gevirtz and Friedman, 1966; Almogi-Labin et al., 1986). We hypothesize biogenic

262   carbonates are dissolved by CO_2 from sedimentary organic matter remineralization, as occurs

263   elsewhere (e.g. Hales and Emerson, 1997; Hales, 2003; Boudreau, 2013), and that high deep Red

264   Sea Ω_C leads to abiotic re-calcification in sediment pores. Morse et al. (2006) find that synthetic

265   high magnesium calcite—unlike biogenic high magnesium calcite—is less soluble than

266   aragonite, so this substitution is favored thermodynamically if the abiotic mineral forms similarly

267   to the synthetic mineral.

268   Calcium carbonate has recently been found as metastable ikaite (a hydrated mineral with

269   the formula $CaCO_3 \cdot 6H_2O$) in natural sea ice (Dieckmann et al., 2008). Ikaite cycling provides

270   a competing explanation for the high Arctic surface *Alk** values if high A_T low-salinity ikaite-

271   rich ice melt becomes separated from low A_T high-salinity rejected brines. However, riverine A_T

272   inputs better explain the magnitude of the feature: The ~5 mg ikaite L^{-1} sea ice that Dieckmann

273   et al. (2008) found in the Antarctic could only enrich A_T of the surface 100 m by ~1 µmol kg^{-1}

274   for each meter of ice melted, and Arctic surface 100 m *Alk** is elevated by 59 µmol kg^{-1} relative

275   to the deeper Arctic in our gridded dataset. By contrast, Jones et al. (2008) estimate a ~5%

276   average riverine end-member contribution to the shallowest 100 m of this region, which accounts

277   for ~55 µmol kg^{-1} *Alk** enrichment. Also, surface *Alk** in the Southern Ocean—which has sea

278   ice but lacks major rivers—is not similarly elevated relative to surface phosphate (Fig. 2) or deep

279   *Alk** (Fig. 3).

280

281   **4. Controls on the calcite saturation state**

282   The *Alk** tracer provides an opportunity to estimate the impact of carbonate cycling on

283   Ω_C. In addition to (1) carbonate cycling, Ω_C is affected by (2) organic matter cycling, (3)

284   freshwater cycling, (4) pressure changes on seawater, (5) heating and cooling, and (6) A_T

285   changes from nitrogen fixation and denitrification. For each of these six processes, we estimate

286   the standard deviation of the net influence of the process globally by considering the standard

287   deviation of a "reference" tracer R_i for the process, "σ_{R_i}", where R_i is *Alk** for CaCO$_3$ cycling,

288   phosphate for organic matter cycling, salinity for freshwater cycling, pressure for pressure

289   changes, temperature for heating and cooling, and *N** (Gruber and Sarmiento, 1997) for nitrogen

290   fixation and denitrification. We use the standard deviation of the reference tracer as a measure

291   of the oceanic range of the net influence of the corresponding process. We measure the impact

292   of this range on Ω_C using a metric *M*, which we define as:

293
$$M_i = \sigma_{R_i} \left| S_{R_i} \right| \tag{6}$$

294   where S_{R_i} is the Ω_C sensitivity to a unit process change in R_i, which we estimate in Appendix A.

295   We are interested in the relative importance *I* of our 6 processes, so we also calculate the

296   percentage that each metric value estimate contributes to the sum of all 6 metric value estimates:

297
$$I_i = 100\% \times \frac{M_i}{\sum_{i=1}^{6} M_i}$$
(7)

298   We derive and estimate our metric and its uncertainty in Appendix A. We carry out our analysis

299   for the full water column assuming it to be isolated from the atmosphere (section 4.1), and also

300   for just the top 50 m of the water column assuming it to be well-equilibrated with the atmosphere

301   (section 4.2). Finally, we consider how equilibration with an atmosphere with a changing pCO$_2$

302   alters surface Ω_C.

303

304   *4.1 Process importance in atmospherically-isolated mean seawater from all ocean depths*

305   Our metric M_i is an estimate of the standard deviation of the global distribution of Ω_C

306   resulting from the ith process. Our relative process importance metric I_i is an estimate of the

307   percentage of overall variability of the Ω_C distribution that can be attributed to that process. We

308   provide M and I values for mean seawater from the full water column alongside the R_i, S_{R_i}, and

309   σ_{R_i} values used to estimate them in Table 1. These calculations assume that the seawater is

310   isolated from the atmosphere.

311   Relative process importance estimates I indicate organic matter cycling (48%) is the

312   dominant process controlling Ω_C for mean seawater. Changing pressure (28%) is the second

313   most important process, followed by calcium carbonate cycling (17%), temperature changes

314   (4%), nitrogen fixation and denitrification (1.21%), and freshwater cycling (0.78%).

315

316   *4.2 Process importance in well-equilibrated surface seawater*

317   In Table 2 we provide M_i values for well-equilibrated seawater in the top 50 m of the

318   ocean alongside the R_i, σ_{R_i}, S_{R_i} used to estimate them. These surface seawater M_i values are

319   calculated assuming the water remains equilibrated with an atmosphere with 400 µatm pCO$_2$.

320   We test the validity of this assumption by also estimating M for the observed global pCO$_2$

321   variability in the Takahashi et al. (2009) global data product. This test reveals transient air-sea

322   disequilibria are indeed important for surface ocean Ω_C, but only as a secondary factor when

323   considered globally. Despite this, it is important to recognize that air-sea equilibration following

324   a process is not instantaneous, and that the S_{R_i} value estimates in section 4.1 may be better for

325   estimating short term changes following fast acting processes such as spring blooms (e.g. Tynan

326   et al., 2014) or upwelling events (e.g. Feely et al., 1988). We omit the disequilibrium M value

327   estimate from the denominator of Eq. (7) to allow I values for surface seawater to be compared

328   to I values from mean seawater globally.

329   Warming and cooling are the dominant processes controlling Ω_C for well-equilibrated

330   surface seawater (76%). The large increase in M for warming and cooling relative to the value

331   calculated for mean seawater is due to lower equilibrium C_T at higher temperatures. Freshwater

332   cycling is the second most important process (13%), followed by carbonate cycling (8%),

333   organic matter cycling (2%), pressure changes (1%), and denitrification and nitrogen fixation

334   (0.4%). The increased importance of freshwater cycling compared to section 4.1 is because

335   freshwater dilutes C_T by more than the equilibrium C_T decreases from A_T dilution, so carbon

336   uptake tends to follow freshwater precipitation and carbon outgassing follows evaporation.

337   Carbonate cycling is less important because A_T decreases with carbonate precipitation lead to

338   lower C_T at equilibrium. Organic matter cycling is much less important because atmospheric re-

339   equilibration mostly negates the large changes in C_T. Pressure changes are negligible because

340   we only consider water in the surface 50 m. Our air-sea disequilibrium M estimate suggests

341   surface disequilibria are comparably important to freshwater cycling for surface Ω_C but

342   substantially less important than temperature changes (this would correspond to an I value of

343   ~14%).

344   The dominance of warming and cooling and freshwater cycling over carbonate cycling is

345   most evident in the Red Sea where high temperatures (>25 °C) and high salinities (>40) lead to

346   surface Ω_C exceeding 6 despite extremely low $Alk*$ (<−200 µmol kg^{-1}). The deep Red Sea is

347   also unusual for having deep water that was warm when it last left contact with the atmosphere

348   (the Red Sea is >20 °C at >1000 m depth). This provides high initial deep Ω_C that—combined

349   with decreased influence of pressure changes at higher temperatures—keeps deep Red Sea Ω_C >

350   3. Similarly, the lowest surface Ω_C values are in the Arctic where there are low temperatures,

351   low salinity, and high $Alk*$ from riverine inputs. The importance of warming and cooling is also

352   suggested by the correlation between global surface Ω_C and the surface temperature ($R^2 = 0.96$).

353   These properties are plotted in Fig. 8.

354

355   **5. Conclusions**

356         $Alk*$ isolates the portion of the A_T signal that varies in response to calcium carbonate

357   cycling and exchanges with terrestrial and sedimentary environments from the portion that varies

358   in response to freshwater and organic matter cycling. The salinity normalization we use has the

359   advantage over previous salinity normalizations that it allows our tracer to mix linearly and to

360   change in a 2:1 ratio with C_T in response to carbonate cycling. We highlight the following

361   insights from $Alk*$:

362   *(1) Alk* distribution*: The $Alk*$ distribution clearly shows the influence of biological

363   cycling including such features as the very low *Alk** in the Red Sea due to the high calcium

364   carbonate precipitation there. We also find evidence of strong riverine A_T sources in the Bay of

365   Bengal and in the Arctic. We show river inputs likely dominate over the small influences of

366   ikaite cycling on the Arctic alkalinity distribution.

367   *(2) Influence of calcium carbonate cycling on marine calcite saturation state*: *Alk** allows

368   us to quantify the net influence of calcium carbonate cycling on marine Ω_C. For well-

369   equilibrated surface waters, carbonate cycling is less influential for Ω_C than gas exchange driven

370   by warming and cooling and freshwater cycling. At depth, the carbonate cycling signal is

371   smaller than the signal from organic matter cycling and from pressure changes. Temperature is

372   the dominant control on Ω_C of surface waters in equilibrium with the atmosphere. This accounts

373   for the low calcite saturation states in the cold surface of the Arctic and Southern Oceans despite

374   high regional *Alk**, and high Ω_C in the warm subtropics despite low regional *Alk**.

375   We intend to use *Alk** for two future projects. First, *Alk** is superior to A_T for monitoring

376   and modeling changes in marine chemistry resulting from changes in carbonate cycling with

377   ocean acidification. A_T varies substantially in response to freshwater cycling, so *Alk** trends may

378   be able to be detected sooner and more confidently attributed to changes in calcium carbonate

379   cycling than trends in A_T (Ilyina et al., 2009). Secondly, we will estimate global steady state

380   *Alk** distributions using *Alk** sources and sinks from varied biogeochemical ocean circulation

381   models alongside independent water mixing and transport estimates (e.g. Khatiwala et al., 2005;

382   Khatiwala, 2007). We will interpret findings in the context of two hypotheses proposed to

383   explain evidence for calcium carbonate dissolution above the aragonite saturation horizon: (1)

384   that organic matter remineralization creates undersaturated microenvironments that promote

385   carbonate dissolution in portions of the water column which are chemically supersaturated in

386 bulk, and (2) that high-magnesium calcite and other impure minerals allow chemical dissolution

387 above the saturation horizon.

388

389 **Acknowledgements**

395

396 **References**

397 Almogi-Labin, A., B. Luz, and J. Duplessy (1986), Quaternary paleo-oceanography, pteropod

398   preservation and stable-isotope record of the Red Sea, *Palaeogeogr., Palaeoclimateol.,*

399   *Palaeoecol.*, *57*, 195-211, doi: 10.1016/0031-0182(86)90013-1.

400 Anderson, L. A. and J. L. Sarmiento (1994), Redfield ratios of remineralization determined by

401   nutrient data analysis*, Global Biogeochem. Cycles, 8*, 65-80, doi: 10.1029/93GB03318.

402 Azetsu-Scott, K., A. Clarke, K. Falkner, J. Hamilton, E. P. Jones, C. Lee, B. Petrie, S.

403   Prinsenberg, M. Starr, and P. Yeats (2010), Calcium carbonate saturation states in the waters

404   of the Canadian Arctic Archipelago and the Labrador Sea, *J. Geophys. Res. Oceans, 115*,

405   C11. doi: 10.1029/2009JC005917.

406 Beldowski, J., A. Löffler, B. Schneider, and L. Joensuu (2010), Distribution and biogeochemical

407   control of total CO_2 and total alkalinity in the Baltic Sea, *J. Mar. Sys., 81*, 252-259.

408   doi:10.1016/j.jmarsys.2009.12.020.

409   Berelson, W. M., W. M. Balch, R. Najjar, R. A. Feely, C. Sabine, and K. Lee (2007), Relating

410   estimates of $CaCO_3$ production, export, and dissolution in the water column to measurements

411   of $CaCO_3$ rain into sediment traps and dissolution on the sea floor: A revised global

412   carbonate budget, *Global Biogeochem. Cycles, 21*, GB1024, doi: 10.1029/2006GB002803.

413   Boudreau, B. P. (2013), Carbonate dissolution rates at the deep ocean floor, *Geophys. Res. Lett.*,

414   *40*, 1-5, doi: 10.1029/2012GL054231.

415   Brewer, P. G., and D. Dyrssen (1985), Chemical oceanography of the Persian Gulf. *Prog.*

416   *Oceanogr.*, *14*, 41-55, doi:10.1016/0079-6611(85)90004-7.

417   Brewer, P. G., G. T. F. Wong, M. P. Bacon, D. W. Spencer (1975), An oceanic calcium

418   problem? *Earth and Planet. Sci. Lett., 26* (1), 81-87, doi: 10.1016/0012-821X(75)90179-X.

419   Cai, W.-J. X. Guo, C. A. Chen, M. Dai, L. Zhang, W. Zhai, S. E. Lohrenz, K. Yin, P. J. Harrison,

420   Y. Wang (2008), A comparative overview of weathering intensity and HCO_3^- flux in the

421   world's major rivers with emphasis on the Changjiang, Huanghe, Zhujiang (Pearl) and

422   Mississippi Rivers, *Contental Shelf Res.*, *28*, 1538-1549, doi:10.1016/j.csr.2007.10.014.

423   Chen, C.-T. A. (2002), Shelf-vs. dissolution-generated alkalinity above the chemical lysocline,

424   *Deep Sea Res. II, 49* (24–25), 5365-5375, doi: 10.1016/S0967-0645(02)00196-0.

425   Cooley, S. R., V. J. Coles, A. Subramaniam, and P. P. Yager (2007), Seasonal variations in the

426   Amazon plume-related atmospheric carbon sink, *Global Biogeo. Chem. Cycles.*, *21* (3),

427   GB3014, doi: 10.1029/2006GB002831.

428   Craig, H., and K.K. Turekian (1980), The GEOSECS program 1976-1979, *Earth Planet. Sci.*

429   *Lett.*, *49*, 263-265, doi: 10.1016/j.bbr.2011.03.031.

430   Dai, A. and K. E. Trenberth (2002), Estimates of freshwater discharge from continents: latitudi-

431   nal and seasonal variations, *J. Hydrometeorology*, *3*, 660-687,

432   doi: http://dx.doi.org/10.1175/1525-7541(2002)003<0660:EOFDFC>2.0.CO;2.

433   Dickson, A.G. (1981), An exact definition of total alkalinity and a procedure for the estimation

434   of alkalinity and total inorganic carbon from titation data, *Deep Sea Res. A*, *28 (6)*, 609-623,

435   doi: 10.1016/0198-0149(81)90121-7.

436   Dickson, A. G. and F. J. Millero (1987), A comparison of the equilibrium constants for the

437   dissociation of carbonic acid in seawater media. *Deep-Sea Res. A, 34*, 1733-1743,

438   doi:10.1016/0198-0149(87)90021-5.

439   Dieckmann, G.S., G. Nehrke, S. Papadimitriou, J. Göttlicher, R. Steininger, H. Kennedy, D.

440   Wolf-Gladrow, and D. N. Thomas (2008), Calcium carbonate as ikaite crystals in Antarctic

441   sea ice. *Geophys. Res. Lett.* , *35*, LO8051, doi:10.1029/2008GL033540.

442   Feely, R. A., C. L. Sabine, K. Lee, F. J. Millero, M. F. Lamb, D. Greeley, J. L. Bullister, R. M.

443   Key, T. H. Peng, and A. Kozyr (2002), In situ calcium carbonate dissolution in the Pacific

444   Ocean. *Global Biogeochem. Cycles, 16*, 1144, doi: 10.1029/2002GB001866.

445   Feely, R. A., R.H. Byrne, J. G. Acker, P. R. Betzer, C. A. Chen, J. F. Gendron, and M. F. Lamb

446   (1988), Winter-summer variations of calcite and aragonite saturation in the northeast

447   Pacific. *Mar. Chem.* 25, *3,* 227-241, doi:10.1016/0304-4203(88)90052-7.

448   Fofonof, N. P., and R. C. Millard (1983), Algorithms for computations of fundamental properties

449   of seawater. UNESCO Technical Papers in Marine Science No. 44, 53 pp.

450   Gascard, J. C., G. Raisbeck, S. Sequeira, F. Yiou, and K. Mork (2004), Correction to 'The

451   Norwegian Atlantic Current in the Lofoten basin inferred from hydrological and tracer

452   data(I-129) and its interaction with the Norwegian Coastal Current'. *Geophys. Res.*

453   *Lett.*, *31*(8), doi: 10.1029/2003GL018303.

454   Gascard, J. C., G. Raisbeck, S. Sequeira, F. Yiou, and K. Mork (2004), Correction to

455   2003GL01803*, Geophys. Res. Lett., 31,* L08302, doi:10.1029/2004GL020006, 2004.

456   Gevirtz, J. L., and G. M. Friedman (1966), Deep-Sea carbonate sediments of the Red Sea and

457   their implications on marine lithification, *J. Sed. Petrol.*, *36*, 143-151.

458   Gruber, N., and J. L. Sarmiento (1997), Global patterns of marine nitrogen fixation and

459   denitrification, *Global Biogeochem. Cycles*, *11*(2), 235-266, doi: 10.1029/97GB00077.

460   Hales, B. (2003), Respiration, dissolution, and the lysocline. *Paleoceanogr.*, *18*(4), 1099, doi:

461   10.1029/2003PA000915.

462   Hales, B., and S. Emerson (1997), Calcite dissolution in sediments of the Ceara Rise: In situ

463   measurements of porewater O_2, pH, and CO_2 (aq). *Geochim. Cosmochim. Acta*, *61*(3), 501-

464   514, doi:10.1016/S0016-7037(96)00366-3.

465   Honjo, S., S. J. Manganini, R. A. Krishfield, and R. Francois (2008), Particulate organic carbon

466   fluxes to the ocean interior and factors controlling the biological pump: A synthesis of global

467   sediment trap programs since 1983, *Prog. Oceanogr.*, *76*(3), 217-285,

468   doi:10.1016/j.pocean.2007.11.003.

469   Ilyina, T. R. E. Zeebe, E. Maier-Reimer, and C. Heinze (2009), Early detection of ocean

470   acidification effects on marine calcification, *Global Biogeochem. Cycles*, *23,* GB1008, doi:

471   10.1029/2008GB003278.

472   Jiang, Z. P., T. Tyrrell, D.J. Hydes, M. Dai, and S.E. Hartman (2014), Variability of alkalinity

473   and the alkalinity-salinity relationship in the tropical and subtropical surface ocean. *Global

474   Biogeochem. Cycles,* *28*(7), 729-742, doi: 10.1002/2013GB004678.

475   Jones, E. P., L. G. Anderson, S. Jutterström, L. Mintrop, and J. H. Swift (2008), Pacific

476   freshwater, river water and sea ice meltwater across Arctic Ocean basins: Results from the

477   2005 Beringia Expedition, *J. Geophys. Res. Oceans*, *113*(C8), doi: 10.1029/2007JC004124.

478   Kanamori, S. and H. Ikegami (1982), Calcium-alkalinity relationship in the North Pacific, *J.*

479   *Oceanogr., 38*, 57-62, doi: 10.1007/BF02110291

480   Kaushal, S. S., G. E. Likens, R. M. Utz, M. L. Pace, M. Grese, and M. Yepsen (2013), Increased

481   river alkalinization in the Eastern U.S., *Envi. Sci. Tech.*, *47*, 10302-10311, doi:

482   10.1021/es401046s.

483   Key, R. M., A. Kozyr, C. L. Sabine, K. Lee, R. Wanninkhof, J. L. Bullister, R. A. Feely, F. J.

484   Millero, C. Mordy, and T. H. Peng (2004), A global ocean carbon climatology: Results from

485   Global Data Analysis Project (GLODAP), *Global Biogeochem. Cycles, 18*, GB4031, doi:

486   10.1029/2004GB002247.

487   Key, R. M., T. Tanhua, A. Olsen, M. Hoppema, S. Jutterström, C. Schirnick, S. van Heuven, X.

488   Lin, D. Wallace and L. Mintrop (2009), The CARINA data synthesis project: Introduction

489   and overview, *Earth Sys. Sci. Data, 2(1),* 579-624, doi:10.5194/essdd-2-579-2009.

490   Khatiwala, S., M. Visbeck, and M. A. Cane, (2005), Accelerated simulation of passive tracers in

491   ocean circulation models, *Ocean Modelling*, *9*(1), 51-69, doi:10.1016/j.ocemod.2004.04.002.

492   Khatiwala, S. (2007), A computational framework for simulation of biogeochemical tracers in

493   the ocean, *Global Biogeochemical Cycles*, *21*(3), GB3001, doi: 10.1029/2007GB002923.

494   Mehrbach, C., C. H. Culberson, J. E. Hawley, and R. M. Pytkowicz (1973), Measurement of the

495   apparent dissociation constants of carbonic acid in seawater at atmospheric pressure, *Limnol.*

496   *Oceanogr., 18*, 897-907.

497   Millero, F. J., K. Lee, and M. Roche, (1998), Distribution of alkalinity in the surface waters of

498   the major oceans, *Marine Chemistry, 60*, 111-130, doi:10.1016/S0304-4203(97)00084-

499   4.Milliman, J. D., D. A. Ross, and T. L. Ku (1969), Precipitation and lithification of deep-sea

500   carbonates in the Red Sea, *J. Sed Res.*, *39*(2), 724-736, doi: 10.1306/74D71CFD-2B21-

501   11D7-8648000102C1865D.

502   Morse, J. W., A. J. Andersson, F. T. Mackenzie (2006), Initial responses of carbonate-rich shelf

503   sediments to rising atmospheric pCO_2 and "ocean acidification": Role of high Mg-calcites.

504   *Geochim. Cosmochm. Acta., 70* (23), 5814-5830, doi:10.1016/j.gca.2006.08.017.

505   Moore, W. S. (2010), The effect of submarine groundwater discharge on the ocean. *Marine Sci.*,

506   *2*, 59-88, doi: 10.1146/annurev-marine-120308-081019

507   Moore, W. S., J. L. Sarmiento, and R. M. Key (1986), Tracing the Amazon component of surface

508   Atlantic water using [228]Ra, salinity, and silica. *J. Geophys. Res.*, *91* (*C2*), 2574-2580,

509   doi: 10.1029/JC091iC02p02574.

510   Orr, J. C., V. J. Fabry, O. Aumont, L. Bopp, S. C. Doney, R. A. Feely, A. Gnanadesikan, N.

511   Gruber, A. Ishida, F. Joos, R. M. Key, K. Lindsay, E. Maier-Reimer, R. Matear, P. Monfray,

512   A. Mouchet, R. G. Najjar, G. Plattner, K. B. Rodgers, C. L. Sabine, J. L Sarmiento, R.

513   Schlitzer, R. D. Slater, I. J. Totterdell, M. Weirig, Y. Yamanaka, and A. Yool, (2005),

514   Anthropogenic ocean acidification over the twenty-first century and its impact on calcifying

515   organisms. *Nature, 437,* 681-686, doi:10.1038/nature04095.

516   Robbins, P. E. (2001), Oceanic carbon transport carried by freshwater divergence: Are salinity

517   normalizations useful?. *J. Geophys. Res*, *106*(C12), 30939-30, doi: 10.1029/2000JC000451.

518   Sarmiento, J. L., J. Dunne, A. Gnanadesikan, R.M. Key, K. Matsumoto, R. Slater (2002), A new

519   estimate of the $CaCO_3$ to organic carbon export ratio. *Global Biogeochem. Cy.*, *16*(4), 1107,

520   doi: 10.1029/2002GB001919.

521   Sarmiento, J. L., N. Gruber, M. A. Brzezinski, and J. P. Dunne (2004), High-latitude controls of

522   thermocline nutrients and low latitude biological productivity. *Nature*, *427*(6969), 56-60,

523   doi:10.1038/nature02127.

524 Silverman, J. B. Lazar, and J. Erez (2007), Effect of aragonite saturation, temperature, and

525   nutrients on the community calcification rate of a coral reef, *J. Geophys. Res.*, *112*,

526   CO05004, doi: 10.1029/2006JC003770.

527 Suzuki, T., M. Ishii, M. Aoyama, J. R. Christian, K. Enyo, T. Kawano, R. M. Key, N. Kosugi, A.

528   Kozyr, L. A. Miller, A. Murata, T. Nakano, T. Ono, T. Saino, K. Sasaki, D. Sasano, Y.

529   Takatani, M. Wakita and C. Sabine (2013), PACIFICA Data Synthesis Project.

530   ORNL/CDIAC-159, NDP-092. Carbon Dioxide Information Analysis Center, Oak Ridge

531   National Laboratory, U.S. Department of Energy, Oak Ridge, Tennessee.

532   doi:10.3334/CDIAC/OTG.PACIFICA_NDP092.

533 Takahashi, T., S. C. Sutherland, R. Wanninkhof, C. Sweeney, R. A. Feely, D. W. Chipman, B.

534   Hales, G. Friederich, F. Chavez, C. Sabine, A. Watson, D. C. E. Bakker, U. Schuster, N.

535   Metzl, H. Yoshikawa-Inoue, M. Ishii, T. Midorikawa, Y. Nojiri, A. Körtzinger, T. Steinhoff,

536   M. Hoppema, J. Olafsson, T. S. Arnarson, B. Tilbrook, T. Johannessen, A. Olsen, R.

537   Bellerby, C. S. Wong, B. Delille, N. R. Bates, and J. W. deBarr, (2009), Climatological mean

538   and decadal change in surface ocean pCO_2, and net sea–air CO_2 flux over the global

539   oceans, *Deep Sea Res. II*, *56*(8), 554-577, doi:10.1016/j.dsr2.2008.12.009.

540 Thomas, H., Y. Bozec, H. J. De Baar, K. Elkalay, M. Frankignoulle, L. S. Schiettecatte, G.

541   Kattner, and A. V. Borges (2005), The carbon budget of the North Sea. *Biogeosci.*, *2*(1), 87-

542   96, doi: 10.5194/bg-2-87-2005.

543 Tynan, E., T. Tyrrell, and E. P. Achterberg (2014), Controls on the seasonal variability of

544   calcium carbonate saturation states in the Atlantic gateway to the Arctic Ocean. *Mar. Chem.*

545   158 (2014) 1-9, doi: 10.1016/j.marchem.2013.10.010.

546 van Heuven, S., D. Pierrot, E. Lewis, and D. Wallace (2009), MATLAB Program developed for

547   CO_2 system calculations*, ORNL/CDIAC-105b, Carbon Dioxide Information Analysis Center,*

548   *Oak Ridge National Laboratory, US Department of Energy, Oak Ridge, Tennessee.*

549   Velo, A., F. F. Perez, P. Brown, T. Tanhua, U. Schuster, and R. M. Key (2009), CARINA

550   alkalinity data in the Atlantic Ocean, *Earth Syst. Sci. Data*, *1*, 45-61, doi:10.5194/essd-1-45-

551   2009.

552   de Villiers, S. (1998), Excess dissolved calcium in the ocean: a hydrothermal hypothesis, *Earth*

553   *and Plan. Sci. Lett.*, *164(3-4)*, 624-641, doi:10.1016/S0012-821X(98)00232-5.

554   Wolery, T. J., and N. H. Sleep (1988), Interactions of geochemical cycles with the mantle. In:

555   Gregor, C. B., R. M. Garrels, F. T. Mackenzie, and J. B. Maynard (eds) Chemical cycles in

556   the evolution of the earth. Wiley, New York, 77-103.

557   Wolf-Gladrow, D. A., R. E. Zeebe, C. Klaas, A. Körtzinger, and A. G. Dickson (2007), Total

558   alkalinity: The explicit conservative expression and its application to biogeochemical

559   processes. *Marine chemistry*, *106*(1), 287-300, doi:10.1016/j.marchem.2007.01.006.

560   Yamamoto-Kawai, M., F. A. McLaughlin, E. C. Carmack, S. Nishino, and K. Shimada (2009),

561   Aragonite undersaturation in the Arctic Ocean; effects of ocean acidification and sea ice

562   melt, *Science, 326*, 1098, doi:10.1126/science.1174190.

563   **Appendix A: Definition of the process importance metric M**

564   In simplest terms, our metric is the product of the Ω_C sensitivity to a process and the

565   variability of the net influence of the process globally. The difficulty in this calculation lies in

566   quantifying the "net influence of a process." We first show how we change coordinates so we

567   can use reference tracers as a proxy measurement for these net influences.

568   Our metric for Ω_C variability resulting from the ith process is expressed as M_i:

$$M_i = \sigma_{P_i} \left| \frac{\partial \Omega_C}{\partial P_i} \right| \tag{A1}$$

570   where P_i is an abstract variable representing the net process influence (that we will later factor

571   out), and $\dfrac{\partial \Omega_C}{\partial P_i}$ is the Ω_C sensitivity to the process. We expand $\dfrac{\partial \Omega_C}{\partial P_i}$ using the chain rule to

572   include a term for Ω_C sensitivity to changes in the reference tracer R_i (see section 4) and a term

573     $\dfrac{\partial R_i}{\partial P_i}$ representing changes in R_i resulting from the ith process:

$$\frac{\partial \Omega_C}{\partial P_i} = \frac{\partial \Omega_C}{\partial R_i} \frac{\partial R_i}{\partial P_i} \tag{A2}$$

575   In practice, we calculate Ω_C as a function of $j = 7$ properties: (1) pressure, (2)

576   temperature, (3) salinity, (4) phosphate, (5) silicate, (6) A_T, and (7) C_T for mean seawater and

577     $p\mathrm{CO}_2$ for surface seawater, so we use the chain rule again to expand the $\dfrac{\partial \Omega_C}{\partial R_i}$ terms as follows:

$$\frac{\partial \Omega_C}{\partial R_i} = \sum_{j=1}^{7} \frac{\partial \Omega_C}{\partial X_j} \frac{\partial X_{j,i}}{\partial R_i} \tag{A3}$$

579   Here, the $\dfrac{\partial X_{j,i}}{\partial R_i}$ are assumed terms (assumptions detailed shortly) that relate the effect of the ith

580   process on the *j*th property to the effect of the process on R_i, and the $\dfrac{\partial \Omega}{\partial X_j}$ terms reflect Ω_C

581   sensitivity to changes in the *j* properties used to calculate it.

582   We make assumptions regarding the $\dfrac{\partial X_{j,i}}{\partial X_R}$ terms: we relate changes in temperature from

583   sinking or shoaling to changes in pressure using the potential temperature (θ) routines of

584   Fofonoff and Millard (1983); we assume freshwater cycling linearly concentrates A_T, C_T,

585   phosphate, and silicate by the same ratio that it changes salinity; we relate C_T, phosphate, and A_T

586   changes from organic matter formation to changes in phosphate using the remineralization ratios

587   found by Anderson and Sarmiento (1994) and the empirical relationship of Kanamori and

588   Ikegami (1982); we also use Kanamori and Ikegami (1982)'s constant to relate changes in A_T

589   from nitrogen fixation and denitrification to changes in N* from these processes; and we assume

590   that an increase in A_T from calcium carbonate dissolution equals the *Alk** increase, and that the

591   corresponding increase in C_T equals half of this *Alk** increase. We neglect any changes in C_T

592   from denitrification and nitrogen fixation because these changes are better thought of as organic

593   matter cycling occurring alongside nitrogen cycling.

594   We estimate $\dfrac{\partial \Omega}{\partial X_j}$ property sensitivity terms as the differences between Ω_C calculated

595   before and after augmenting *j*th property by 1 unit. Ω_C is calculated with the MATLAB

596   CO2SYS routines written by van Heuven et al. (2009) using the carbonate system equilibrium

597   constants of Mehrbach et al. (1973), as refit by Dickson and Millero (1987). Seawater $p\mathrm{CO}_2$ is

598   used in place of C_T for the surface seawater calculations (when $j = 7$) to calculate the change in

599   Ω_C that remains after the surface seawater is allowed to equilibrate with the atmosphere.

600   We assume that the distributions of our R_i reference properties are linearly related to the

601   P_i net activities of their associated processes. This assumption implies:

602
$$\sigma_P = \sigma_{R_i} \left| \frac{\partial P_i}{\partial R_i} \right| \tag{A4}$$

603   We can then substitute Eq. (A3) into Eq. (A2), and substitute this combined equation for $\dfrac{\partial \Omega_C}{\partial P_i}$

604   and (A4) into Eq. (A1). We then cancel the $\dfrac{\partial P_i}{\partial R_i}$ and $\dfrac{\partial R_i}{\partial P_i}$ terms to obtain:

605
$$M_i = \sigma_{R_i} \left| \sum_{j=1}^{7} \frac{\partial \Omega_C}{\partial X_j} \frac{\partial X_{j,i}}{\partial R_i} \right| \tag{A5}$$

606   We then define Ω_C sensitivity S_{R_i} as:

607
$$S_{R_i} = \left| \sum_{j=1}^{7} \frac{\partial \Omega_C}{\partial X_j} \frac{\partial X_{j,i}}{\partial R_i} \right| \tag{A6}$$

608   where S_{R_i} is the Ω_C sensitivity to a change in the ith process scaled to a unit change in the

609   reference variable for that process. We can then substitute Eq. (A6) into Eq. (A5) to obtain Eq.

610   6. We use Eqn. (A6) to define S_{R_i} and Eqn. 6 to calculate M. We provide the $\dfrac{\partial \Omega_C}{\partial X_j}$ and $\dfrac{\partial X_{j,i}}{\partial R_i}$
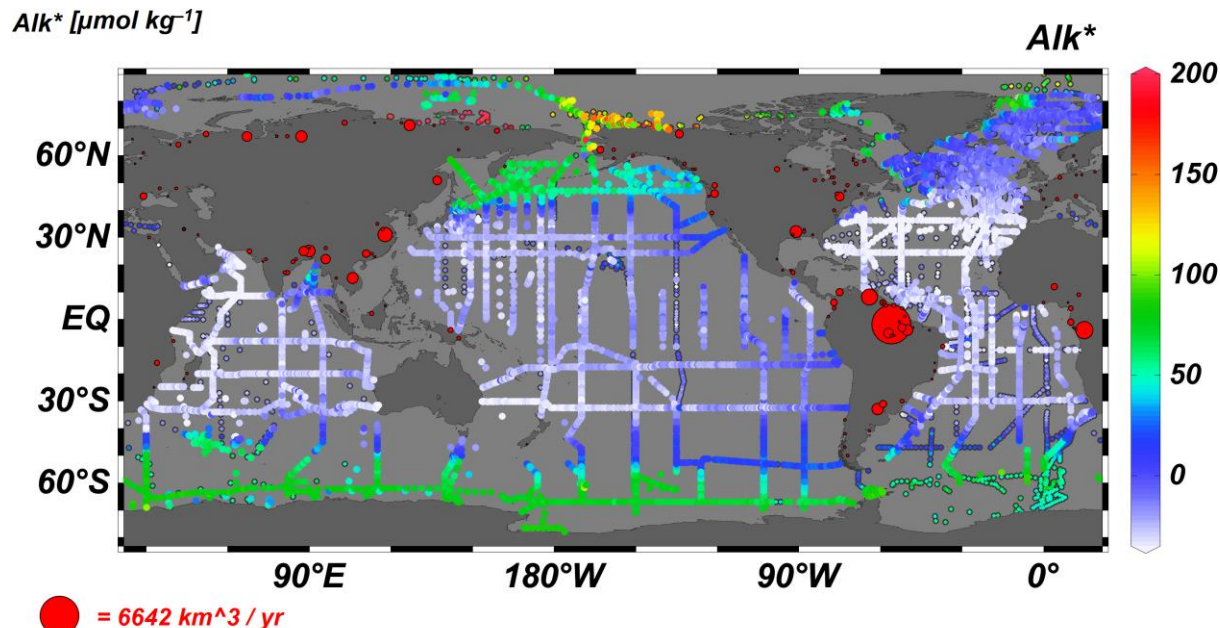
611   values we use to estimate S_{R_i} for atmospherically isolated seawater from all depths in Table A1

612   and for well-equilibrated surface seawater in Table A3. We perform a sample I and M

613   calculation in Supplementary Materials document SE.

614   We use a Monte Carlo analysis to estimate variability and uncertainty in our metric M

615   and our percent relative process importance I calculations. We calculate the standard deviations,

616   σ_M and σ_I, of pools of 1000 M and I estimates calculated after adjusting the seawater properties

617   X_i with a normally-distributed perturbation with a standard deviation equal to the property

618   standard deviation from the gridded dataset. We find $\dfrac{\sigma_I}{I}$ is typically much smaller than $\dfrac{\sigma_M}{M}$.

619   This is because Ω_C sensitivity is typically proportional to the Ω_C itself, so individual Monte

620   Carlo M estimates vary with the initial Ω_C and one another. Our σ_M estimates are therefore

621   better thought of as measures of the ranges of sensitivities found in the modern ocean, while σ_I

622   represent variability in the relative importance of processes. We provide σ_M and σ_I for

623   atmospherically isolated seawater globally in Table A2, and for well-equilibrated surface
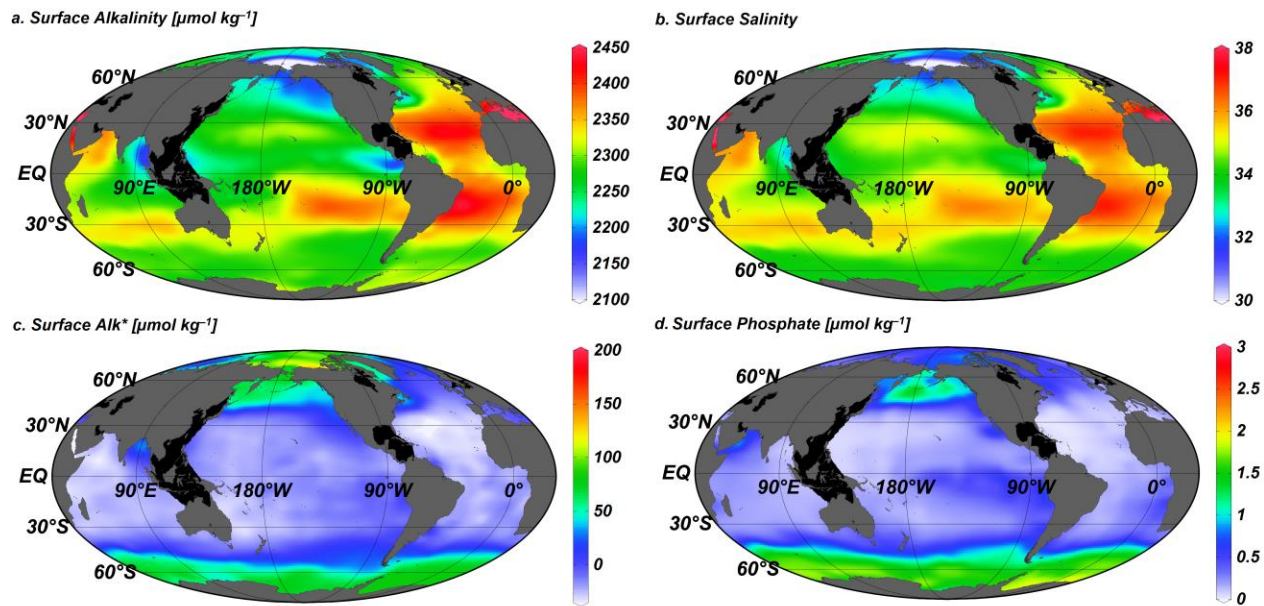
624   seawater in Table A4.

625

626

Figure 1. A map of station locations at which we use measurements to estimate *Alk** (in μmol kg^{-1}). Dot color indicates surface *Alk**. Points with black borders indicate that either A_T was measured prior to 1992 (i.e. before reference materials were commonly used) or that no nitrate value was reported (in which case a nitrate concentration of 5 μmol kg^{-1} is assumed). Red dots on land indicate the mouth locations and mean annual discharge volumes (indicated by dot size) of 200 large rivers, as given by Dai and Trenberth (2002).

627

628

629

630

Figure 2. Global (a) total alkalinity A_T, (b) salinity, (c) *Alk**, and (d) phosphate distributions at the surface (10 m depth surface) from our gridded CARINA, PACIFICA, and GLODAP bottle data product detailed in Supplementary Materials document SA. Areas with exceptionally poor coverage in the data used to produce the gridded product are blacked out.
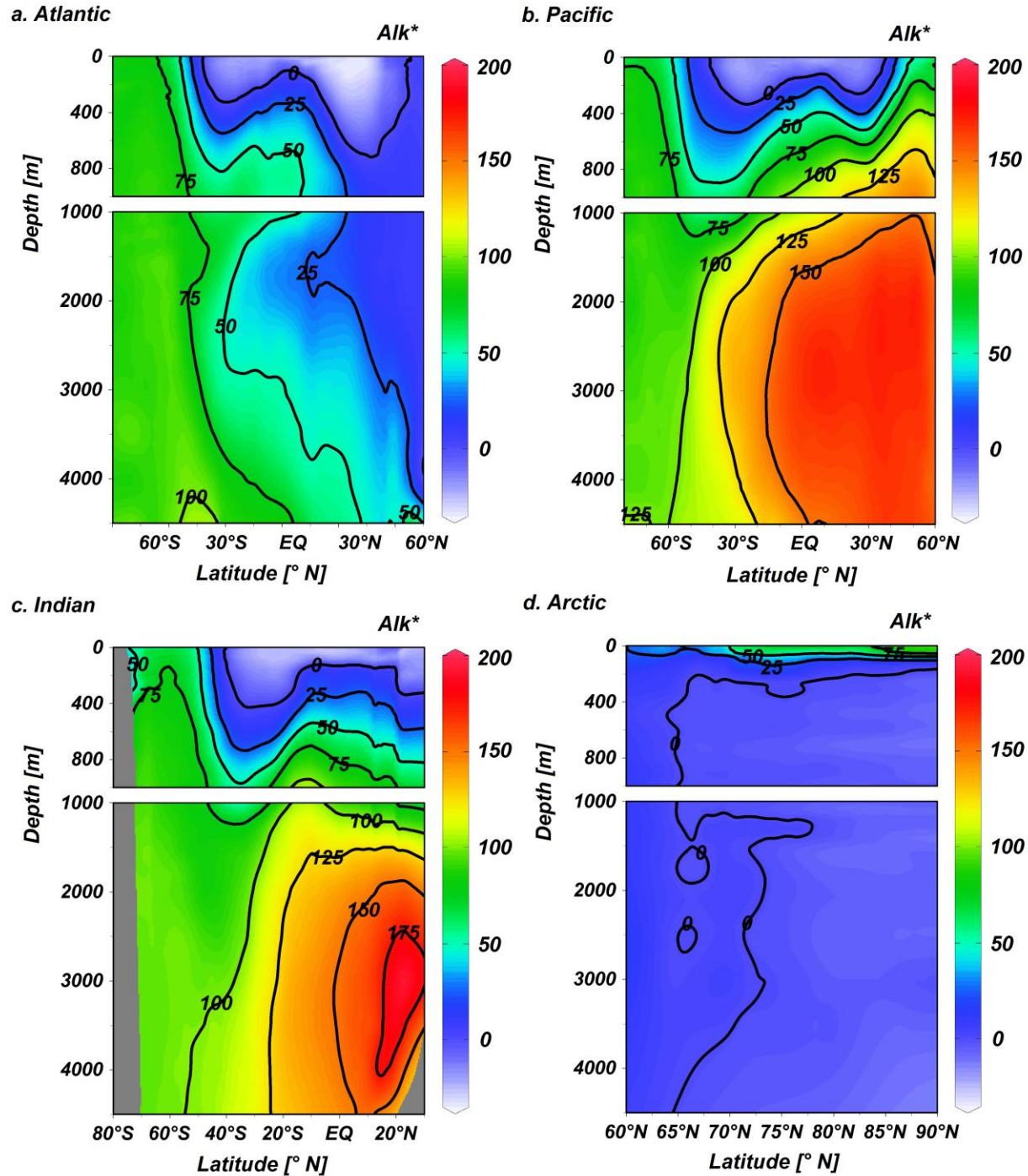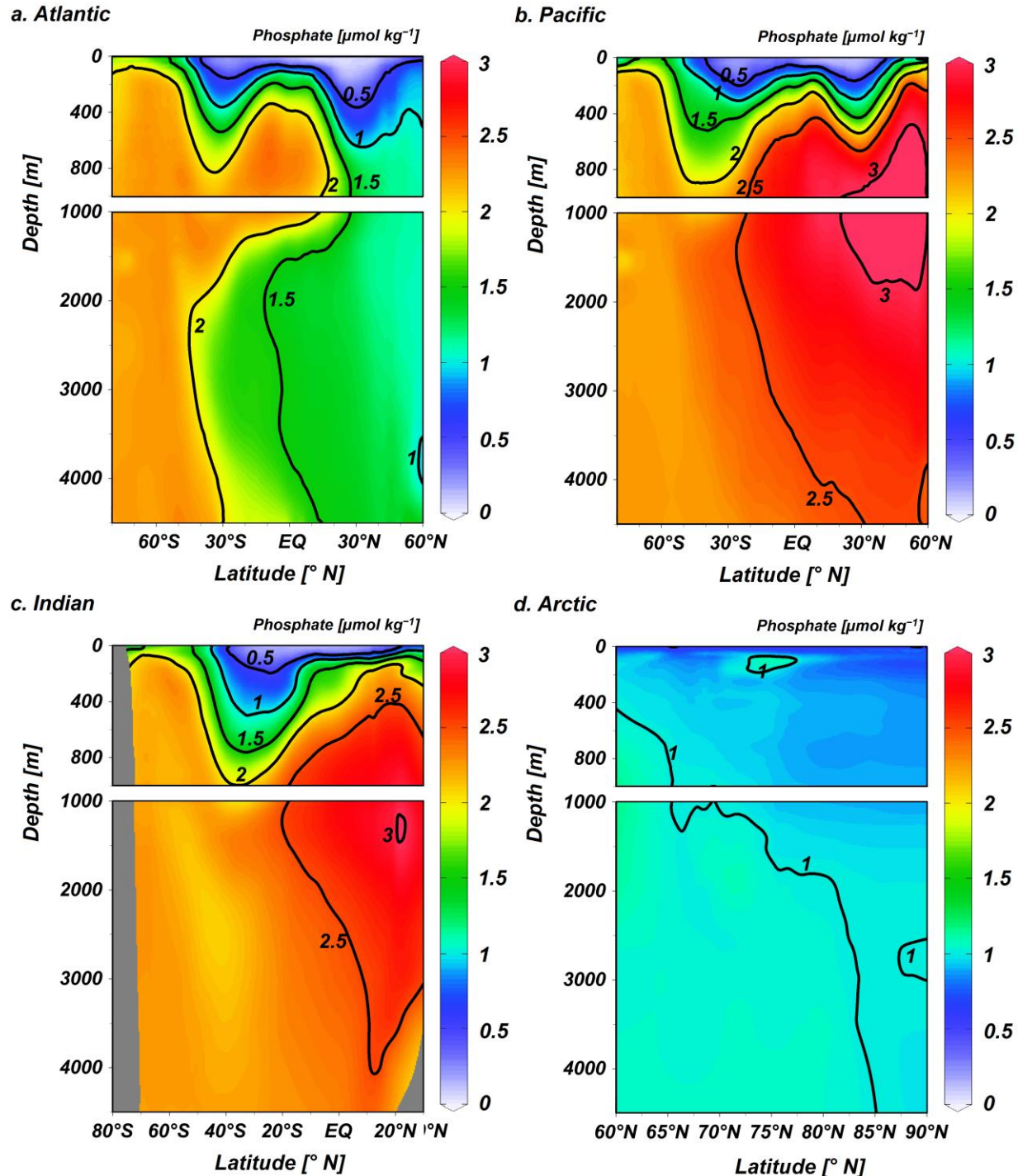
631

632

633

634

635

636

637

638

Figure 3. Zonal mean gridded *Alk** (in μmol kg⁻¹) in the (a) Atlantic, (b) Pacific, (c) Indian, and (d) the Arctic oceans plotted against latitude and depth.

639
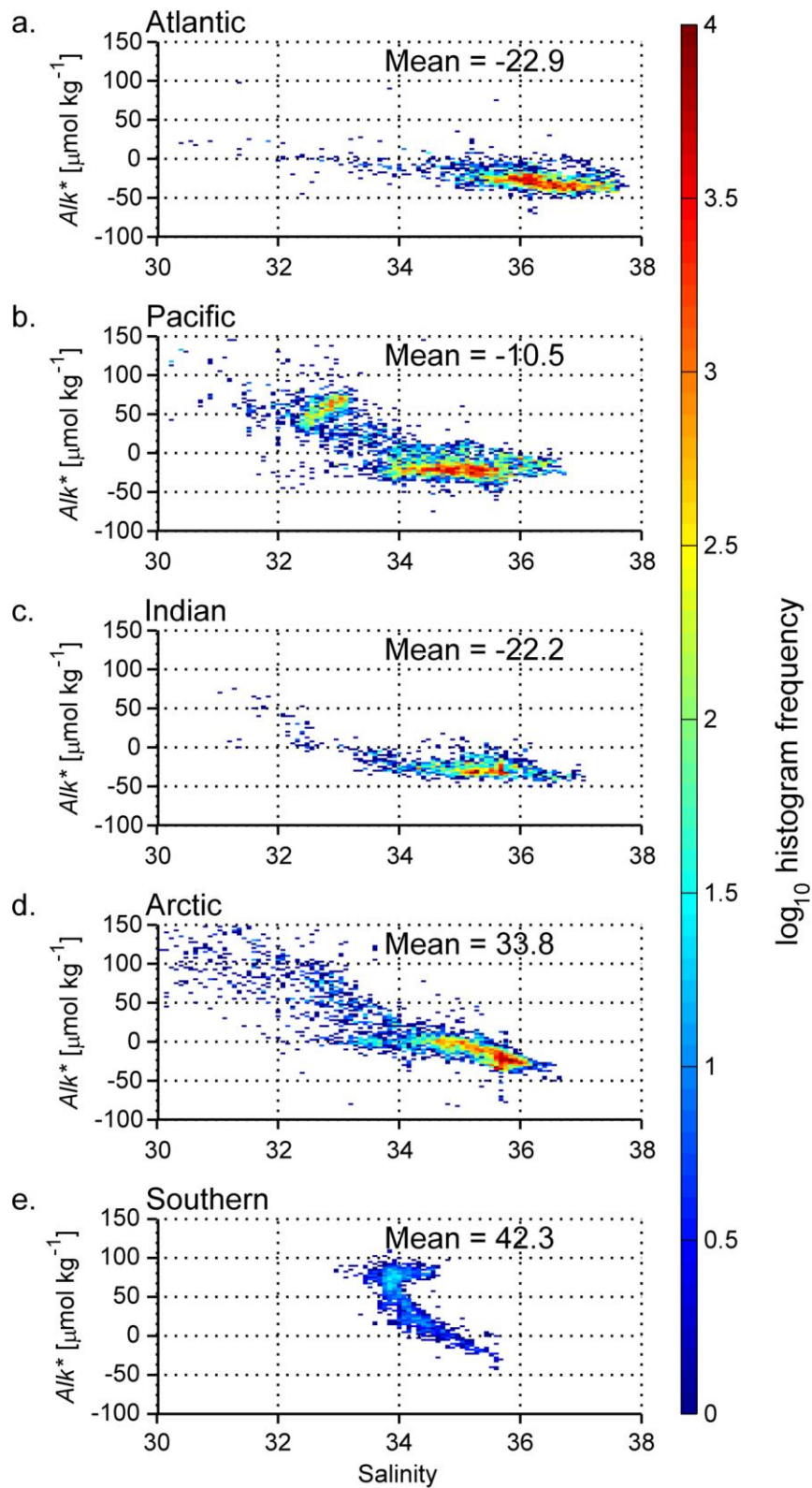
Figure 4. Zonal mean gridded phosphate (in μmol kg^{-1}) in the (a) Atlantic, (b) Pacific, (c) Indian, and (d) the Arctic oceans plotted against latitude and depth.
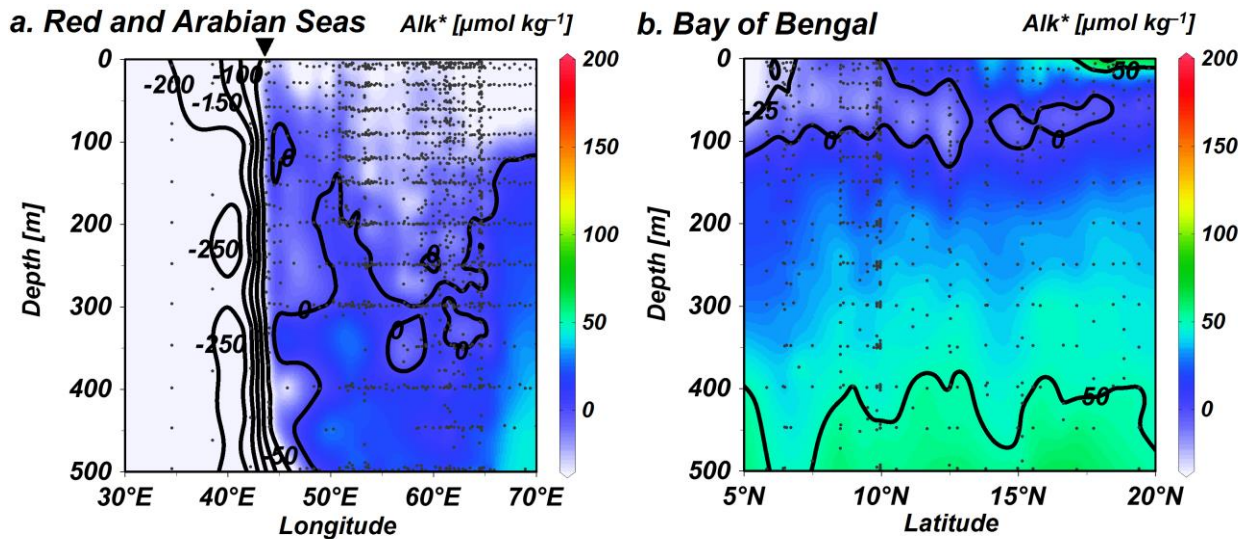
640

641

642

Figure 5. 2-D histograms indicating the log (base 10) of the number of measurements that fall within bins of *Alk** vs. salinity with color. Data are limited to the top 50 m of the (a) Atlantic, (b) Pacific, (c) Indian, (d) Arctic, and (e) Southern Oceans. Where basins connect, the boundary between the Atlantic and the Arctic oceans is 40°N, between the Atlantic and the Indian is 20° E,
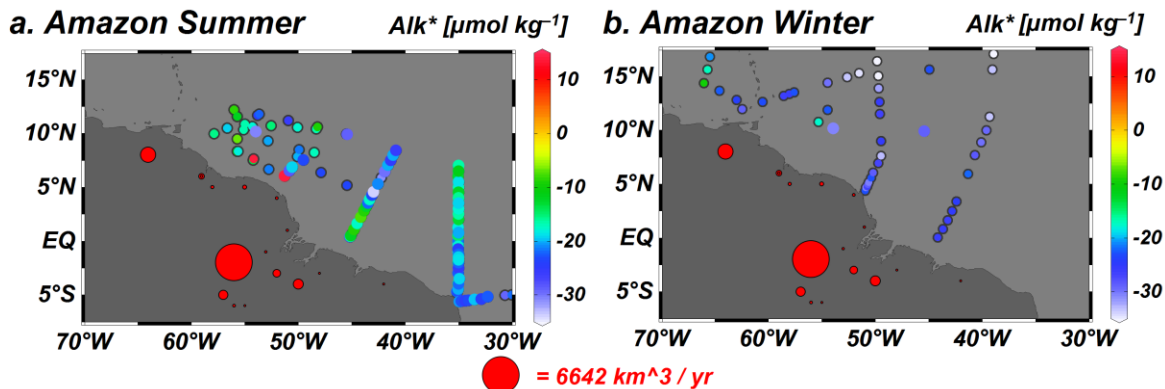
between the Indian and the Pacific is 131° E, between the Pacific and the Atlantic is 70° W, and between the Southern Ocean and the other oceans is 40°S.

643

Figure 6. *Alk** distributions (in μmol kg^{-1}) (a) between 5° and 30°N in the Red and Arabian Seas shown against longitude, and (b) between 75° and 100° E in the Bay of Bengal plotted against latitude. Small black dots indicate where data is present. The inverted triangle above (a) indicates the longitude of the mouth of the Red Sea.

644

Figure 7. *Alk** (in μmol kg^{-1}) in top 50 m of the ocean near the Amazon River outflow plotted in color, though with a narrower color scale than is used for all other plots. Panel (a) is limited to data collected in November through January, and in panel (b) is limited to measurements from May through July. Points with black borders indicate that either the A_T was measured prior to 1992 (before reference materials were commonly used) or that no nitrate value was reported (in which case a nitrate concentration of 5 μmol kg^{-1} is assumed). Red dots on land indicate the mouth locations and mean annual discharge volumes (indicated by dot size) of large rivers, as given by Dai and Trenberth (2002).

645
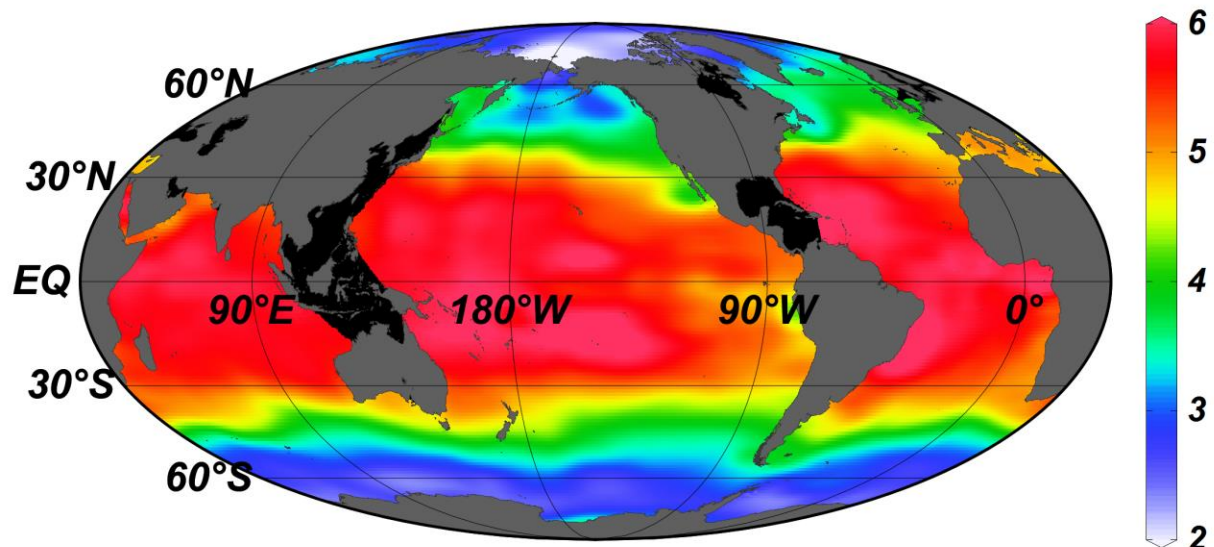
646
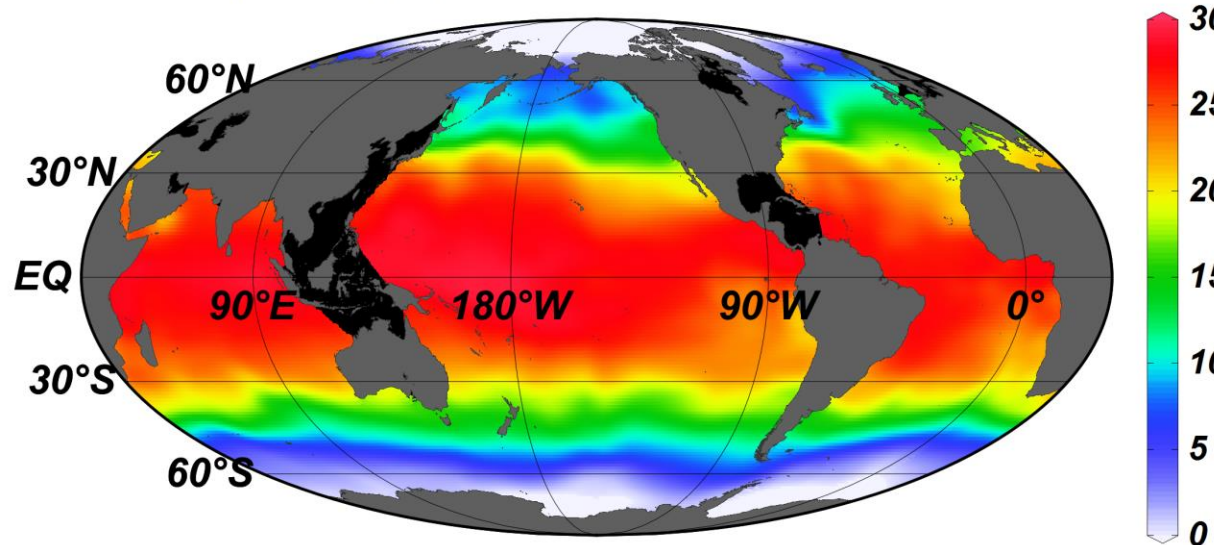
647

648

a. Surface Calcite Saturation

b. Surface Temperature [°C]

Figure 8. Gridded global (a) calcite saturation state Ω_C, and (b) temperature at the surface (10 m depth surface) of our gridded CARINA, PACIFICA, and GLODAP bottle data product. Areas with exceptionally poor coverage in the data used to produce the gridded product are blacked out.

649

650

651

652

653

654

Table 1. Metric estimates M_i, relative process importance percentages I_i, Ω_C sensitivities S_{R_i} to unit changes in the R_i reference properties, and reference property standard deviations σ_{R_i} for the $i = 6$ processes in atmospherically isolated mean seawater from all ocean depths. See Appendix A for details on how these terms are estimated and explanation of how M_i and I_i uncertainties are obtained.

Process	i	R_i	S_{R_i}	σ_{R_i}	M_i	I_i
Carbonate cycling	1	*Alk**	0.0043	53.5 μmol/kg	0.23	17%
Org. matter cycling	2	Phosphate	−0.0069	0.60 μmol/kg	0.66	48%
Freshwater cycling	3	Salinity	0.032	0.27	0.011	0.78%
Sinking / shoaling	4	Pressure	−0.00028	1411 db	0.4	28%
Warming / cooling	5	Temp.	0.014	4.20 °C	0.06	4%
Denit./nit. fix.	6	N*	−0.010	1.6 μmol/kg	0.017	1.2%

655

656

657

Table 2. Metric estimates M_i, relative process importance percentages I_i, Ω_C sensitivities S_{R_i} to unit changes in the R_i reference properties, and reference property standard deviations σ_{I_i} for the $i = 6$ processes in well-equilibrated surface seawater. See Appendix A for details on how these terms are estimated and explanation of how M_i and I_i uncertainties are obtained.

Process	i	R_i	S_{R_i}	σ_{R_i}	M_i	I_i
Carbonate cycling	1	*Alk**	0.0034	36.9 µmol/kg	0.13	7.8%
Org. matter cycling	2	Phosphate	−0.0045	0.51 µmol/kg	0.037	2.3%
Freshwater cycling	3	Salinity	0.20	0.86	0.22	13.2%
Sinking / shoaling	4	Pressure	−0.00083	15 db	0.011	0.70%
Warming / cooling	5	Temp.	0.14	8.8 °C	1.2	76%
Denit ./ nit. fix.	6	N*	−0.0043	1.5 µmol/kg	0.006	0.40%
*p*CO₂ disequilibria	†	pCO₂	−0.0086	27 µatm*	0.23	†

* standard deviation of the Takahashi et al. (2009) revised global monthly *p*CO₂ climatology

† the *M* value for disequilibria is only calculated to test our assumption of surface seawater air-sea equilibration, and is omitted from calculations of I_i for comparison with Table 1.

658

659

660

Table A1. $\dfrac{\partial \Omega_C}{\partial X_j}$ (bold text) and $\dfrac{\partial X_{j,i}}{\partial R_i}$ (italic text) terms used in Eq. (A5) for atmospherically isolated mean seawater from all ocean depths. These terms are specific to the $j = 7$ (columns) properties we use to calculate Ω_C and $i = 6$ (rows) processes we consider. Units for $\dfrac{\partial \Omega_C}{\partial X_j}$ are the inverse of the listed X_j units. Units for $\dfrac{\partial X_{j,i}}{\partial R_i}$ are the X_j units divided by the R_i units given in Table 1.

Properties		Pressure	Temp	Salinity	Phos.	Silicate	A_T	C_T
X_j units		db	°C		μmol/kg	μmol/kg	μmol/kg	μmol/kg
j		1	2	3	4	5	6	7
Mean seawater values		2235	3.7	34.71	2.15	49.0	2362	2254
$\dfrac{\partial \Omega_C}{\partial X_j}$		**–0.00028**	**0.014**	**–0.011**	**–0.0085**	**–0.00012**	**0.0082**	**–0.0079**
		$\dfrac{\partial X_{1,i}}{\partial R_i}$	$\dfrac{\partial X_{2,i}}{\partial R_i}$	$\dfrac{\partial X_{3,i}}{\partial R_i}$	$\dfrac{\partial X_{4,i}}{\partial R_i}$	$\dfrac{\partial X_{5,i}}{\partial R_i}$	$\dfrac{\partial X_{6,i}}{\partial R_i}$	$\dfrac{\partial X_{7,i}}{\partial R_i}$
Process	*i*							
Carbonate cycling	1	-	-	-	-	-	*1*	*0.5*
Org. matter cycling	2	-	-	-	*1*	-	*–20.16*	*117*
Freshwater cycling	3	-	-	*1*	*0.062*	*1.4*	*68*	*65*
Sinking / shoaling	4	*1*	*0.00010*	-	-	-	-	-
Warming / cooling	5	-	*1*	-	-	-	-	-
Denit ./ nit. fix.	6	-	-	-	-	-	*–1.26*	-

661

662

663

664

Table A2. Monte Carlo derived estimates for M_i variability (σ_{M_i}) and I_i variability (σ_{I_i}) for atmospherically-isolated mean seawater from all ocean depths.

Process	i	σ_{M_i}	σ_{I_i}
Carbonate cycling	1	0.09	1%
Org. matter cycling	2	0.2	3%
Freshwater cycling	3	0.006	0.08%
Sinking / shoaling	4	0.2	5%
Warming / cooling	5	0.02	2%
Denit. / nit. fix.	6	0.006	0.1%

665

666

667

Table A3. $\dfrac{\partial \Omega_C}{\partial X_j}$ (bold text) and $\dfrac{\partial X_{j,i}}{\partial R_i}$ (italic text) terms used in Eq. (A5) for well-equilibrated surface seawater. These terms are specific to the $j = 7$ (columns) properties we use to calculate Ω_C and $i = 6$ (rows) processes we consider. Units for $\dfrac{\partial \Omega_C}{\partial X_j}$ are the inverse of the listed X_j units. Units for $\dfrac{\partial X_{j,i}}{\partial R_i}$ are the X_j units divided by the R_i units given in Table 2.

Properties	Pressure	Temp	Salinity	Phos.	Silicate	A_T	$p\mathrm{CO}_2$
units	db	°C		μmol/kg	μmol/kg	μmol/kg	μatm
j	1	2	3	4	5	6	7
Mean seawater values	25	18.3	34.82	0.51	2.5	2305	350
$\dfrac{\partial \Omega_C}{\partial X_j}$	**−0.00084**	**0.14**	**−0.022**	**−0.0038**	**−0.00013**	**0.0034**	**−0.0086**

Process	*i*	$\dfrac{\partial X_{1,i}}{\partial R_i}$	$\dfrac{\partial X_{2,i}}{\partial R_i}$	$\dfrac{\partial X_{3,i}}{\partial R_i}$	$\dfrac{\partial X_{4,i}}{\partial R_i}$	$\dfrac{\partial X_{5,i}}{\partial R_i}$	$\dfrac{\partial X_{6,i}}{\partial R_i}$	$\dfrac{\partial X_{7,i}}{\partial R_i}$
Carbonate cycling	1	-	-	-	-	-	*1*	-
Org. matter cycling	2	-	-	-	*1*	-	*−20.16*	-
Freshwater cycling	3	-	-	*1*	*0.015*	*0.072*	*65.9*	-
Sinking / shoaling	4	*1*	*0.00010*	-	-	-	-	-
Warming / cooling	5	-	*1*	-	-	-	-	-
Denit./nit. fix.	6	-	-	-	-	-	*−1.26*	-

668

669

Table A4. Monte Carlo derived estimates for M_i variability (σ_{M_i}) and I_i variability (σ_{I_i}) for well-equilibrated surface seawater.

Process	i	σ_{M_i}	σ_{I_i}
Carbonate cycling	1	0.03	0.8%
Org. matter cycling	2	0.01	0.2%
Freshwater cycling	3	0.04	0.5%
Sinking / shoaling	4	0.001	0.03%
Warming / cooling	5	0.2	1%
Denit. / nit. fix	6	0.002	0.04%
pCO$_2$ disequilibria	†	0.05	†

† disequilibria are included only as a test of our assumption of surface seawater air-sea equilibration, so these M_i values are omitted from calculations of I

670

671

672